Geometric and electronic structures of $Cs_2BB'X_6$ double perovskites: The importance of exact exchange

Yuyang Ji,[1,2] Peize Lin,[3,4,*] Xinguo Ren,[3,†] and Lixin He[1,2,‡]

[1]*Key Laboratory of Quantum Information, University of Science and Technology of China, Hefei, Anhui, 230026, People's Republic of China*

[2]*Synergetic Innovation Center of Quantum Information and Quantum Physics, University of Science and Technology of China, Hefei, 230026, People's Republic of China*

[3]*Institute of Physics, Chinese Academy of Sciences, Beijing 100190, China*

[4]*Songshan Lake Materials Laboratory, Dongguan 523808, Guangdong, China*

(Received 20 November 2023; revised 18 June 2024; accepted 24 July 2024; published 14 August 2024)

A widely adopted computational protocol in contemporary materials research is to first relax materials' geometries using semilocal density functional approximations (DFA), and then determining their electronic band structures using the more expensive hybrid functionals. This procedure often works well, as the popular semilocal DFAs, such as the Perdew-Burke-Ernzerhof (PBE) generalized gradient approximation, yield rather good geometries for a wide range of materials. However, here we show that, for some of the lead-free halide double perovskites (HDPs) $Cs_2BB'X_6$ ($B = Ag^+$, Na^+; $B' = In^{3+}$, Bi^{3+}; $X = Cl^-$, Br^-), the validity of this common practice is questionable. We find that, for these HDPs, the geometrical structures, in particular, the $B(B')$-X bond lengths predicted by PBE show large deviations from the experimental values. Additionally, the band gaps of some of these materials (specifically, the In-based HDPs) are sensitive to the $B(B')$-X bond lengths. As a consequence, the band gaps obtained using the hybrid functionals (such as the Heyd-Scuseria-Ernzerhof functional) based on the PBE geometries can still be quite off, in particular, for HDPs with $B' = In^{3+}$. The situation is significantly improved by using hybrid functionals with tuned portion of exact exchange, based on the geometries determined consistently under the same level of theory. The successes and failures of several popular exchange-correlation (XC) functionals are traced back to the so-called delocalization error, and can be quantitatively analyzed and understood via a three-atom linear-chain B-X-B' molecular model. Finally, our findings provide a practical guide for choosing appropriate XC functionals for describing HDPs and point to a promising path for band structure engineering via doping and alloying.

DOI: 10.1103/PhysRevResearch.6.033172

I. INTRODUCTION

Hybrid perovskites (HPs) exhibit excellent transport and optical properties, such as high carrier mobility [1], long carrier diffusion lengths [2–5], and strong absorption coefficients [6]. The power conversion efficiency of HP solar cells has reached 26.1% [7]. However, the toxicity and instability issues of HPs still hinder their widespread applications.

Lead-free halide double perovskites (HDPs) with chemical formula $A_2BB'X_6$ have been proposed as environmentally friendly alternatives [8–13] to HPs with long working lifetimes, and they have been applied in various optoelectronic devices, such as LEDs [9,12], photocatalysts [14], and solar cells [15–18]. For most HDPs, A is chosen as a Cs^+ or organic cation with a large ionic radius to stabilize the crystal structure, while X represents a halide ion. B and B' are occupied by monovalent and trivalent elements, respectively, such as Ag^+, Na^+ and Bi^{3+}, In^{3+}. Compared to conventional HPs, most HDPs have large band gaps which limit their applications in the visible light region. The band structures can be engineered by chemical substitution, alloying, and doping strategies [9,10,12,13,19]. Density functional theory (DFT) is a powerful tool to study the geometric and electronic structures of these materials, and therefore may provide useful guidance for band-structure engineering of HDPs.

The Perdew-Burke-Ernzerhof (PBE) generalized gradient approximation (GGA) functional [20] is one of the most widely used functionals for calculating the structural and electronic properties of HDPs. However, it usually underestimates the band gaps substantially, which is characteristic of the Kohn-Sham (KS) scheme under local and semilocal approximations. Hybrid functionals mixed with a portion of exact exchange are able to reduce the many-body self-interaction (or delocalization) errors and, thanks to the generalized KS scheme, produce band gaps in much better agreement with experimental values. Furthermore, many-body perturbation theory (MBPT) formulated under the GW approximation and Bethe-Salpeter equation has been applied to this type of

*Contact author: linpeize@sslab.org.cn
†Contact author: renxg@iphy.ac.cn
‡Contact author: helx@ustc.edu.cn

material [9,21,22], which is considered to be capable of providing start-of-the-art accuracy for electronic and optical properties. In previous first-principles calculations, the electronic structures of the HDPs calculated by hybrid functionals and/or MBPT are usually performed using the geometries obtained by the PBE functional [15,19,23,24]. Such a strategy, although computationally efficient, may be unreliable, as in some cases the delocalization errors can alter the potential energy surface substantially, leading to inaccurate geometries [25]. Furthermore, it has been shown that the electronic structures of HDP can be sensitive to their geometries [8,10,11]. Understanding the effect of delocalization errors on the geometries of HDPs and, subsequently, on their band structures, will help us choose more appropriate computational protocols.

In this paper, we systematically investigate the geometrical and electronic properties of five HDPs ($Cs_2AgInCl_6$, $Cs_2NaInCl_6$, $Cs_2AgBiCl_6$, $Cs_2AgBiBr_6$, and $Cs_2NaBiCl_6$) using several popular functionals (PBE, PBEsol [26], DFT+U [27], strongly constrained and appropriately normed functional [28], and screened hybrid HSE-type functionals with different mixing parameters [29,30]). We quantitatively assess the size of the delocalization errors in terms of an error function, based on which we find that the sensitivity of electronic structure of HDPs to the bond length indeed stems from the delocalization errors. Among these functionals, only hybrid functionals mixed with an appropriate amount of exact exchange can yield reliable geometries. This analysis provides a practical guide for a DFT user to choose appropriate functionals for studying and designing HDPs.

II. METHODS

The DFT calculations in this paper are carried out using the ATOMIC-ORBITAL BASED AB-INITIO COMPUTATION AT USTC (ABACUS) package [31–33]. As mentioned above, to systematically analyze the performance of different types of functionals for the HDP materials, several popular functionals, including PBE, PBEsol [26], DFT+U [27], SCAN [28], and HSE [29,30], with $\alpha = 0.25$ and $\alpha = 0.4$, are used in our calculations. Here, we use different mixing parameters in HSE to investigate the impact of varying ratios of exact exchange on both the geometries and electronic structures. DFT+U [34], SCAN [35], and HSE [36–38] have recently been implemented in ABACUS, based on the numerical atomic orbital (NAO) basis set framework. Hybrid functional calculations are generally much more expensive than semilocal functionals due to the expense of evaluating the exact-exchange component. The canonical scaling for evaluating the exact-exchange contribution is $O(N^4)$, with N being a measure of system size. For NAO basis sets, by exploiting the strict spatial locality of NAOs and the physically decay behavior of density matrix, one can design linear-scaling algorithm for exact-exchange calculations, leading to efficient hybrid functional calculations, as demonstrated in Ref. [37]. This enables routine hybrid functional calculations, including geometry relaxations, for systems containing hundreds of atoms or even larger. Such types of calculations are still rather challenging for standard plane-wave-based implementations that are readily available in the present days. It should be noted that the speedup brought by NAO-based implementation does not come with a sacrifice of numerical accuracy, as demonstrated in Refs. [36,38].

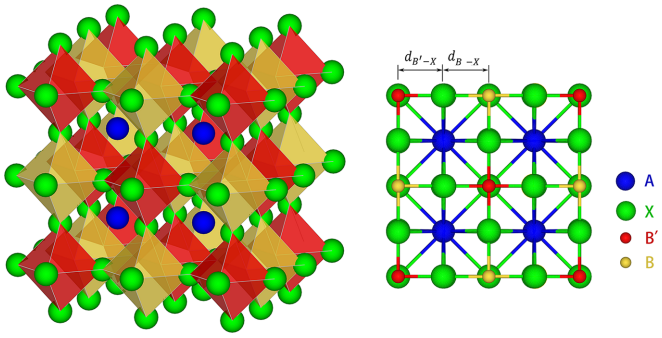

FIG. 1. Crystal structure of $A_2BB'X_6$ with bond lengths d_{B-X} and $d_{B'-X}$. The image on the right provides a frontal view of the HDP crystal structure.

If not stated otherwise, in this paper HSE means the standard HSE with $\alpha = 0.25$, while HSE(0.4) means that HSE with an enlarged mixing parameter $\alpha = 0.4$. For Ag-contained perovskites ($Cs_2AgInCl_6$, $Cs_2AgBiCl_6$, $Cs_2AgBiBr_6$), the DFT+U calculations are performed where a U value of 5.0 eV is adopted for Ag-d orbitals. The spin-orbit coupling (SOC) effect is taken into account in band-structure calculations, when necessary. The high-symmetry path in the Brillouin zone is chosen as L-G-X-W-L-K-G, and the corresponding coordinates are shown in Table S8.

We adopt the SG15 [39] optimized norm-conserving Vanderbilt-type pseudopotentials [40], where the valence electron configurations for different elements are set as follows: Cs : $5s^25p^66s$, Ag: $4s^24p^64d^{10}5s$, In: $4d^{10}5s^25p$, Cl: $3s^23p^5$, Bi: $5d^{10}6s^26p^3$, and Br: $4s^24p^5$. The second-generation NAO bases, namely, the DPSI bases sets [41], are used in all calculations. More specifically, the double-zeta plus polarization NAO basis sets, namely, Cs with $[4s2p1d]$, Ag with $[4s2p2d1f]$, In with $[2s2p2d]$, Cl with $[2s2p1d]$, Na with $[4s2p1d]$, Bi with $[2s2p2d]$, and Br with $[2s2p1d]$, are used. The numerical precision that one can achieve with these optimized NAOs, accessible on the ABACUS website [33], has been extensively tested [41]. Additionally, 100 Ry energy cutoff is used in ABACUS for the Hartree potential calculation and for determining the uniform quadrature grid. An $8 \times 8 \times 8$ Γ-centered Monkhorst-Pack $\boldsymbol{k}$-point mesh is used for self-consistent calculations, and a $12 \times 12 \times 12$ $\boldsymbol{k}$-point mesh is used to calculate the projected density of states (PDOS), which serves to characterize the distribution of electronic states at various energies (states/eV).

III. RESULTS

A. First-principles calculations

Figure 1 depicts the crystal structure of $A_2BB'X_6$ HDPs, which has the $Fm\bar{3}m$ space group symmetry. The B and B' ions are located alternately in the center of the AX_6 octahedra. The B-X (B'-X) bond length, i.e., the distance between B (B') and X in the same octahedral unit is marked as d_{B-X} ($d_{B'-X}$).

We first calculate the lattice constants of the five HDPs using the PBE, HSE, and HSE(0.4), and the obtained results are presented together with the experimental values in

TABLE I. Comparison of the lattice constants a_0 (in Å) obtained by PBE, standard HSE ($\alpha = 0.25$), and HSE with $\alpha = 0.4$ [i.e., HSE(0.4)]. Exp: experimental lattice constants. MAE: mean absolute error. RE: relative error. If there are multiple experimental values, their average value is employed to estimate RE and MAE.

	PBE		HSE		HSE(0.4)		
	a_0	RE	a_0	RE	a_0	RE	Exp
$Cs_2AgInCl_6$	10.678	1.9%	10.631	1.4%	10.564	0.8%	10.481 [8]
$Cs_2NaInCl_6$	10.711	1.8%	10.670	1.4%	10.599	0.7%	10.514 [43], 10.534 [10]
$Cs_2AgBiCl_6$	11.106	3.1%	11.002	2.1%	10.946	1.6%	10.777 [19,44]
$Cs_2AgBiBr_6$	11.447	1.8%	11.440	1.7%	11.380	1.2%	11.250 [45]
$Cs_2NaBiCl_6$	11.036	1.8%	11.028	1.7%	10.966	1.2%	10.839 [46], 10.842 [10]
MAE	0.221		0.180		0.117		

Table I. The lattice constants are determined by fitting to the Birch-Murnaghan [42] equation of states. The mean absolute errors (MAEs) of the lattice constants predicted by the PBE, HSE, and HSE(0.4) with respect to the experimental values are 0.221 Å, 0.180 Å and 0.117 Å, respectively. As can be seen from Table I, the lattice constants obtained via HSE(0.4) are in much better agreement with experiment than those yielded by PBE and HSE.

We then compare the equilibrium bond length d^0_{B-X} as determined by the PBE, HSE, and HSE(0.4) functionals. To reduce the degrees of freedom and to facilitate the comparison with the experimental results, we fix all the lattice constants at the experimental values. As such, the distance between B and its adjacent B' atom is also fixed. We then adjust the position of X atoms along the B-B' direction to alter d_{B-X} and $d_{B'-X}$, resulting in a series of modified geometries. As such, increasing the bond length d_{B-X} means decreasing the bond length $d_{B'-X}$, whereby the symmetry is maintained. We determine the equilibrium bond length according to the minimum of the energy-versus-distance [$E(d)$] curve for each solid as yielded by different functionals.

The equilibrium bond lengths d^0_{B-X} for the five HDPs as determined using the above procedure are listed in Table II, in comparison with the experimental values. It can be seen that PBE significantly underestimates the B-X (with B = Na, Ag) bond lengths [amounting to significantly overestimating the B'-X (B' = In, Bi) bond lengths], yielding a MAE of 0.038 Å. HSE predicts much better B-X bond lengths with a MAE of 0.021 Å, while HSE(0.4) gives the lowest MAE of 0.010 Å. We also check the influence of dispersion corrections, which can improve the description of structural properties in case van der Waals interactions are important. To this end, we perform PBE-D3 [47] calculations and find that the dispersion correction has marginal influence on the determined bond length and lattice constant. For example, for $Cs_2AgInCl_6$, the PBE-D3 lattice constant is 10.654 Å, whereas the PBE value is 10.678 Å, as shown in Table I. Moreover, the Ag-Cl bond length is determined to be 2.683 Å by PBE-D3, whereas the corresponding PBE value is 2.687 Å, as listed in Table II. These results indicate that vdW interactions doesn't play a significant role in HDPs.

To examine how the geometrical structure affects the electronic structure in the HDP materials, we calculate the band gap as a function of the B-X bond length using the aforementioned functionals: PBE, PBEsol, DFT+U, SCAN, HSE, and HSE(0.4). Figure 2(a) presents the results for $Cs_2AgInCl_6$ as an illustrating example, which shows that the calculated band gaps from all functionals, despite being of different sizes, increase linearly with increasing Ag-Cl bond length, d_{Ag-Cl}. As a side remark, our calculations indicate that $Cs_2AgInCl_6$ shows a negligible SOC effect on the band structure and, therefore, we only show the results without including SOC. As can be seen from Fig. 2(a), the band gap given by HSE(0.4) at the PBE Ag-Cl bond length (2.687 Å) is approximately 2.671 eV, which is substantially smaller than the HSE(0.4) band gap obtained at its own Ag-Cl bond length (2.724 Å), 3.023 eV. Obviously, the latter is in much better agreement with the experimental value (3.3 eV), marked by the red triangle in the figure. This result clearly shows that calculating the band gaps using HSE-type functionals on the geometry obtained by the PBE functional, which is a commonly adopted computational procedure, may still significantly underestimate the band gap. PBEsol, a revised PBE functional for solids, yields a similar optimized Ag-Cl bond length (2.684 Å)

TABLE II. Comparison of the equilibrium bond lengths d^0_{B-X} (in Å) obtained by PBE, standard HSE ($\alpha = 0.25$), and HSE with $\alpha = 0.4$ [i.e., HSE(0.4)]. Exp: experimental B-X bond lengths. MAE: mean absolute error. RE: relative error.

	PBE		HSE		HSE(0.4)		
	d^0_{B-X}	RE	d^0_{B-X}	RE	d^0_{B-X}	RE	Exp
$Cs_2AgInCl_6$	2.687	−1.7%	2.709	−0.9%	2.724	−0.3%	2.733 [8]
$Cs_2NaInCl_6$	2.716	−1.2%	2.733	−0.5%	2.745	−0.1%	2.748 [43]
$Cs_2AgBiCl_6$	2.673	−1.3%	2.689	−0.7%	2.696	−0.4%	2.707 [19,44]
$Cs_2AgBiBr_6$	2.771	−1.1%	2.787	−0.6%	2.798	−0.2%	2.803 [45]
$Cs_2NaBiCl_6$	2.708	−1.7%	2.721	−1.2%	2.734	−0.7%	2.754 [46]
MAE	0.038		0.021		0.010		

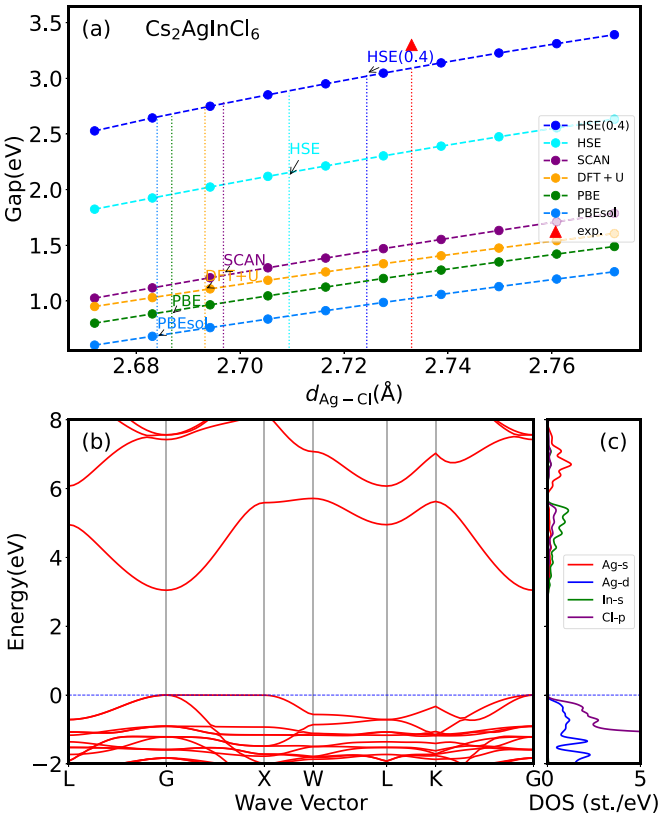

FIG. 2. (a) Band gaps of $Cs_2AgInCl_6$ with a lattice constant of 10.481 Å predicted by HSE(0.4), HSE, SCAN, DFT+U, PBE, and PBEsol as a function of bond length d_{Ag-Cl}. The experimental structure and band gap are obtained from Ref. [8]. (b), (c) Band structure and partial DOS of $Cs_2AgInCl_6$ with d^0_{Ag-Cl} calculated using the HSE(0.4) functional.

as PBE, but slightly smaller band gap (0.682 eV). Moreover, DFT+U calculations were also performed for this system. The DFT+U method introduces an on-site Hubbard U correction to the DFT Hamiltonian and, here, a U value of 5 eV is adopted for the Ag-d orbitals. However, the calculated bond length (2.693 Å) and band gap (1.108 eV) are not appreciably improved compared to PBE. This is understandable, as the major contributions to the band edges of $Cs_2AgInCl_6$ are not of Ag d character, but stem from Cl p and In s orbitals, as can be seen from the partial DOS (PDOS) plot presented in Fig. 2(c). Thus, it is not surprising that applying the Hubbard U correction to the semicore Ag d states does not alter the band gap of $Cs_2AgInCl_6$ significantly.

The recently developed meta-GGA SCAN functional [28] has shown promising performance for a wide range of applications [48,49]. Here we also applied SCAN to calculate the band structure of $Cs_2AgInCl_6$. The obtained SCAN band gap and bond length are noticeably better than the PBE, PBEsol, and DFT+U results, but a severe underestimation of the band gap by more than a factor of 2 persists. Finally, we performed calculations using the standard HSE functional (with $\alpha = 0.25$), and the obtained band gap is halfway between the results obtained by semilocal functionals and that given by HSE(0.4). The HSE band gaps at PBE and HSE optimized bond lengths (2.687 Å and 2.709 Å) are 1.93 eV and 2.14 eV, respectively, yielding a difference of 0.21 eV in the band gaps obtained at these two geometries. This is smaller than the corresponding value of 0.35 eV obtained between the PBE and HSE(0.4) geometries, as it should be. These results reveal that, although it is crucial to incorporate a portion of exact exchange in the functional to yield quantitatively accurate band gaps for HDPs, the proper amount is not *a priori* clear. The default ratio $\alpha = 0.25$ is not always the best choice.

Figure 2(b) shows the band structure of $Cs_2AgInCl_6$ calculated using the HSE(0.4) functional, with d_{Ag-Cl} also determined by HSE(0.4). The corresponding PDOS are shown in Fig. 2(c). The lowest conduction band of $Cs_2AgInCl_6$ is very dispersive, which is dominated by the delocalized Cl 3p and In 5s electrons, but also contains some contributions from the Ag 5s states. The dispersive bands suggest that the electrons have very small effective masses (Table S2), and therefore large carrier mobility, which is good for photoelectronic device applications. The highest VB is much flatter and, in particular, there is a flat band between the Γ and X points. This flat band is composed of Cl 3p and Ag 4d orbitals [Fig. 2(c)] near the Fermi level.

B. Delocalization error analysis

Based on the extensive benchmark results using six representative XC functionals presented above, we conjecture that the high sensitivity of the band gap to the Ag-Cl bond length, and the strong dependence of the determined Ag-Cl bond length on the employed functional, stems from the competition between the Ag-Cl bond and In-Cl bond, as well as the difficulty for the common XC functionals to properly capture the delicate balance between these two bonds. It is highly likely that the latter has an origin in the delocalization error inherent in these functionals. To have a deeper analysis of the underlying driving mechanism, we construct a simple model system, i.e., a linear-chain molecule, Ag-Cl-In, and examine the effect of the delocalization errors of four of the functionals [PBE, SCAN, HSE, and HSE(0.4)] on the geometry and the electronic structure. The length of the molecular chain is 5.2405 Å, equivalent to its value in the bulk, which is half of the experimental lattice constant of $Cs_2AgInCl_6$ [inset of Fig. 3(b)]. Similar to the bulk case, we fix the length of the full molecular chain, but vary the Ag-Cl (and hence the In-Cl) bond lengths and monitor how things change. First, we verify that different functionals perform similarly for the model molecule and for the HDP bulk material, as can be seen from Figs. 3(a) and 3(b), where the total energies as a function of the Ag-Cl bond length are presented, for both the bulk and molecular systems, respectively. For bulk $Cs_2AgInCl_6$, the equilibrium Ag-Cl bond lengths predicted by PBE, SCAN, HSE, and HSE(0.4) are 2.687, 2.697, 2.709, and 2.724 Å, respectively, while for the molecule, the corresponding values are 2.737, 2.765, 2.772, and 2.795 Å, respectively. Thus, for both the bulk system and molecular model, the calculated Ag-Cl bond lengths follow the following sequence: d_{Ag-Cl}[HSE(0.4)]> d_{Ag-Cl}(HSE) > d_{Ag-Cl}(SCAN) > d_{Ag-Cl}(PBE). Obviously, the opposite behavior is true for the In-Cl bond.

An interesting question arising in this context is whether the above-noted functional dependence of the equilibrium

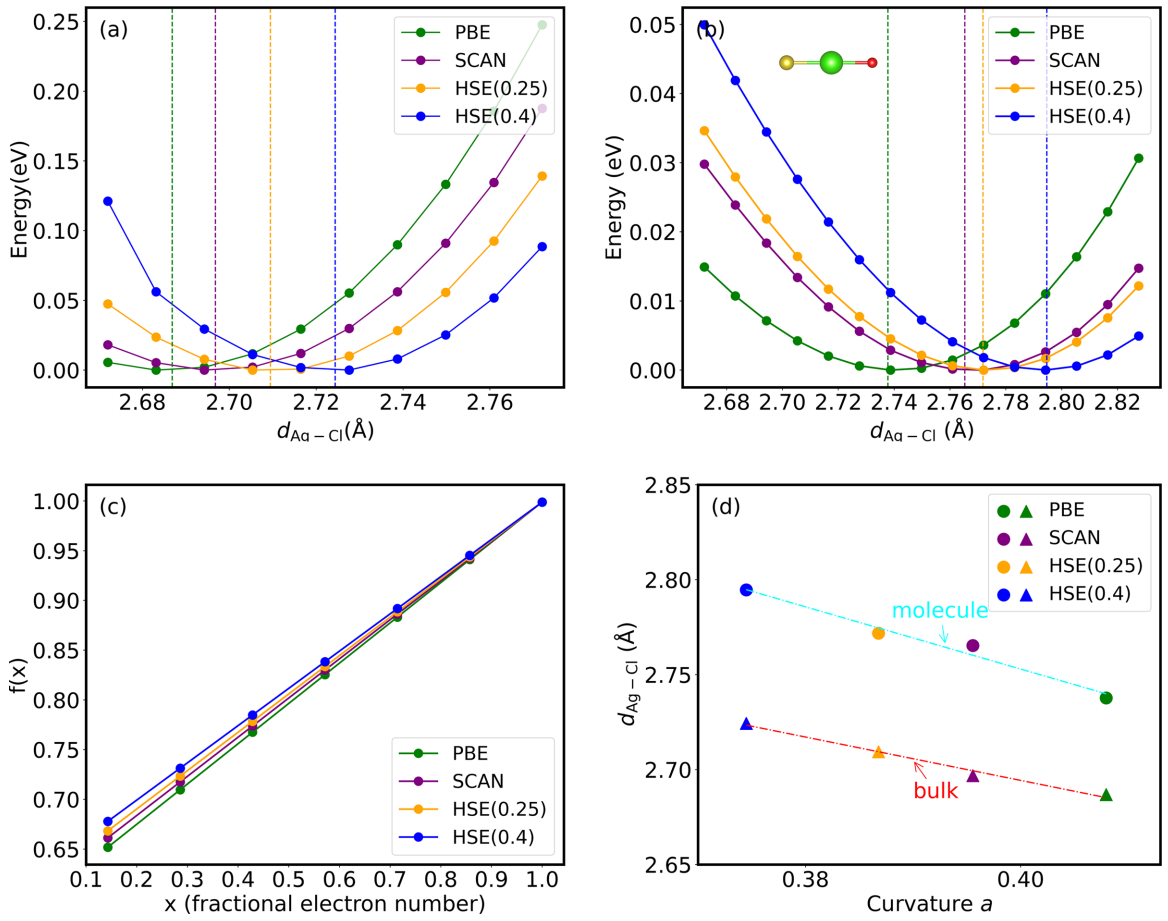

FIG. 3. (a), (b) The total energies of the bulk $Cs_2AgInCl_6$ (a) and the Ag-Cl-In molecular model (b) as a function of the Ag-Cl bond length, as calculated by the PBE (green), SCAN (purple), HSE (orange), and HSE(0.4) (blue) functionals. The inset of (b) depicts the structure of the molecule model. (c) $f(x)$ for fractional ionization of the molecule model at $d_{Ag-Cl} = 2.739$ Å. (d) The equilibrium Ag-Cl bond lengths as determined by the four functionals for both the bulk system and molecular model versus the curvature a.

bond length is rooted in the delocalization error of the individual functionals [50]. To address this question, following Ref. [51], we use a simple function $f(x)$ to quantify the delocalization error, which is defined as

$$E(N-x) = E(N) + xf(x)(E(N-1) - E(N)). \quad (1)$$

It has been proven by Perdew *et al.* [52] that the energy E of a system with $N-x$ electrons (where N is a positive integer and x lies between 0 and 1) is exactly given by the linear interpolation between the energies at N and $N-1$. Thus, the ideal value of $f(x)$ in Eq. (1) is 1. Hait and Head-Gordon [51] found that $f(x)$ is well described by a linear fit of $ax+b$, with $b = 1-a$ as required by the constraint $f(x=1) = 1$. Here we investigate the delocalization errors of PBE, SCAN, HSE, and HSE(0.4) by computing $E(N-x)$ with $0 \leqslant x \leqslant 1$ and thereby determine $f(x)$ for the Ag-Cl-In molecule. The obtained $f(x)$'s for the four functionals as a function of x are plotted in Fig. 3(c), where a linear behavior of $f(x)$ for all the functionals is clearly observed. Here, the slope a of $f(x)$ corresponds to the curvature of $E(N-x)$, and the linear behavior of $f(x)$ means that $E(N-x)$ follows a nearly perfect parabolic behavior as a function of the fractional charge x. Moreover, $a > 0$ corresponds to the convex behavior of $E(N-x)$, implying the presence of a delocalization error, as is the case for all four functionals investigated here. In fact, the magnitude of a can be used as a quantitative measure of the delocalization error of a given functional. In Fig. 3(d), we plot the equilibrium Ag-Cl bond lengths as determined by PBE, SCAN, HSE, and HSE(0.4) for both the bulk system and molecular model versus the curvature a—a measure of the delocalization error—for the four functionals. Remarkably, a nearly linear relationship is observed for both the bulk and molecular systems. This strongly suggests that the functional dependence of the determined equilibrium bond length in $Cs_2AgInCl_6$ is indeed governed by the delocalization error in the employed functionals and, moreover, the underlying driving physics can already be captured by a simple molecular model. Since the model only contains three atoms, and an increase of Ag-Cl bond length means a decrease of the In-Cl, one may well conclude that it is the difficulty for the commonly used functionals to sufficiently capture the competition between the Ag-Cl and In-Cl bonds that renders a first-principles description of HDP materials particularly challenging.

Another interesting aspect that Fig. 2(a) reveals is that the band gap of $Cs_2AgInCl_6$ increases almost linearly as the Ag-Cl bond length increases (or, equivalently, as the In-Cl bond length decreases). In fact, as further shown in Fig. S1(a)

TABLE III. Mulliken charge analysis of the model Ag-Cl-In chain molecule, as obtained by PBE, SCAN, and HSE(0.4) functionals. In our calculations, the neutral Ag, Cl, and In atoms contain 19, 7, and 13 electrons, respectively.

	PBE	SCAN	HSE(0.4)
Ag^{+}	19.069	19.067	19.054
Cl^{-}	7.392	7.396	7.439
In^{3+}	12.539	12.537	12.506

of the Supplemental Material (SM) [53], upon increasing the Ag-Cl bond length, the VBM of $Cs_2AgInCl_6$ of decreases, while the CBM increases almost linearly, resulting in a gradually enlarged band gap. As indicated in the partial DOS plotted in Fig. 2(a), the VBM is mainly composed of Cl 3p states, while the CBM mainly derives from the In 5s states. One can think of the following scenario, namely, as the In-Cl bond shrinks, the hybridization strength between the frontier In 5s and Cl 3p orbitals increases, resulting in an enlarged band gap. Naturally, a counteractive effect occurs between the Ag 3d and Cl 3p states. However, this effect seems to be outweighed by the In-Cl hybridization due to the stronger interaction of the latter. To check the validity of this conjecture, we examined the variation of the HOMO (highest occupied molecular orbital) and LUMO (lowest unoccupied molecular orbital) levels of the Ag-Cl-In linear molecule upon increasing of the Ag-Cl bond length. The results are shown in Fig. S1(b), from which one can see that the change of the HOMO and LUMO levels is very similar to the VBM and CBM of the $Cs_2AgInCl_6$ bulk, as a function of the Ag-Cl (or In-Cl) bond length. This indicates that the variation of the band gap with respect to the Ag-Cl bond length can indeed also be understood from the competition of the Ag-Cl and In-Cl bonds within a simple Ag-Cl-In molecular model, with interaction strength of the In-Cl bond dominating over the Ag-Cl bond. Further evidence comes from the Mulliken charge analysis of the model Ag-Cl-In molecule, as shown in Table III, where one can see the charge transfer between In and Cl atoms is much more pronounced than that between Ag and Cl atoms, for all three functionals, suggesting stronger hybridization between In and Cl than that between Ag and Cl. Moreover, Table III reveals that the charge transfer between In and Cl yielded by the HSE(0.4) functional is slightly stronger than its counterparts given by PBE and SCAN functionals. This is consistent with the fact that the In-Cl bond length determined by HSE(0.4) is shorter than those determined by PBE and SCAN.

C. Other HDP materials

After having thoroughly discussed the geometrical and electronic structures of $Cs_2AgInCl_6$, we turn to other HDP materials. We first briefly discuss $Cs_2NaInCl_6$, which amounts to replacing Ag in $Cs_2AgInCl_6$ by Na. In Fig. S2(a) of the SM, we present the band gap of $Cs_2NaInCl_6$ as a function of the Na-Cl bond length, and find that the overall variation trend of the band gap with respect to the Na-Cl bond length is very similar to that of $Cs_2AgInCl_6$. The partial DOS analysis reveals that the frontier orbitals are almost exclusively of In and Cl characters, i.e., contributions from Na are vanishingly small. This means that the Na-Cl bond plays a less important role in $Cs_2NaInCl_6$ than the Ag-Cl bond in $Cs_2AgInCl_6$. The dependence of the determined Na-Cl and In-Cl bond lengths on the functionals follows a similar pattern as $Cs_2AgInCl_6$. For this material, the measured experimental optical band gaps also show large scatter, with reported values between 3.7 to 4.7 eV [10,43,54,55]. Since the lattice constant used in our calculations is taken from Ref. [43], we also take the experimentally reported gap (4.7 eV) from this paper as the experimental reference value for comparison. It is indicated by the red triangle in Fig. S2(a), which sits in between the theoretical band gaps given by HSE and HSE(0.4). It is worth noting that $Cs_2NaInCl_6$ exhibits a greater exciton binding energy compared to $Cs_2AgInCl_6$ [9,22]. Moreover, electron-phonon and exciton-phonon coupling effects [9,43,55] significantly contribute to the electronic properties of HDP materials, thereby complicating the direct comparison between calculated and experimental results [56].

The next material we would like to analyze is $Cs_2AgBiCl_6$, which is obtained by substituting In in $Cs_2AgInCl_6$ by Bi. A larger change in the band structure is expected, since, compared to $Cs_2AgInCl_6$, $Cs_2AgBiCl_6$ has a larger lattice constant of 10.777 Å and the Bi ion introduces a strong SOC effect. Indeed, different from $Cs_2AgInCl_6$ and $Cs_2NaInCl_6$, $Cs_2AgBiCl_6$ has an indirect band gap. This feature can be correctly described by both PBE and HSE functionals, with or without including SOC. In Fig. 4(a), we plot the (indirect) band gap of $Cs_2AgBiCl_6$ as a function of the Ag-Cl bond length for several different functionals, including PBE, SCAN, DFT+U, PBEsol HSE(0.4). Similar to the case of $Cs_2AgInCl_6$, all functionals, except for HSE(0.4), produce too small band gaps. Moreover, all functionals predict that the band gap increases with increasing Ag-Cl bond length for $Cs_2AgBiCl_6$, although the magnitude of the change is less dramatic, as shown in Fig. 4(a). In analogy with $Cs_2AgInCl_6$, this behavior must stem from the increased hybridization between Bi 6p and Cl 3p states as the Bi-Cl bond shrinks.

The PBE calculated band gap at the HSE(0.4) Ag-Cl bond length is 1.807 eV without including SOC, and decreases to 1.547 eV after SOC is included, indicating the importance of SOC for this materials. Compared to the experimental value of 2.77 eV, PBE significantly underestimates the band gap, regardless of whether the SOC is included or not. The situation also holds for other semilocal functionals. The band gap calculated by the HSE(0.4) functional at the bond length determined by this functional is approximately 3.13 eV without SOC, and 2.63 eV when the SOC is included. The latter is in excellent agreement with the experimental gap marked as the red triangle in Fig. 4(b). For this material, if the HSE(0.4) band gap were calculated using the PBE optimized Ag-Cl bond length, its value would be 0.15 eV smaller.

The band structure of $Cs_2AgBiCl_6$ calculated by HSE(0.4) is shown in Fig. 4(b). Results obtained both with (red solid lines) and without (blue dashed lines) SOC are plotted. In these calculations, the experimental lattice constant is used, and the Ag-Cl bond length is determined using HSE(0.4). As can clearly be seen in Fig. 4(b), the strong SOC of the Bi atoms leads to giant splitting of the low-lying conduction bands, which significantly reduces the band gap.

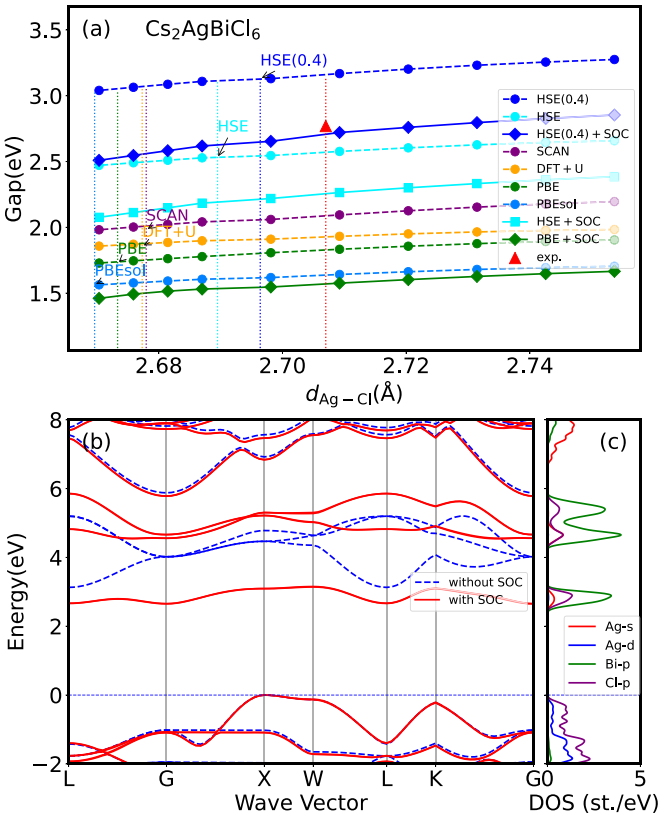

FIG. 4. (a) Band gaps of $Cs_2AgBiCl_6$ with a lattice constant of 10.777 Å predicted by different methods (i.e., HSE(0.4), HSE(0.4)+SOC, SCAN, DFT+U, PBE and PBEsol, and PBE+SOC) as a function of bond length d_{Ag-Cl}. The experimental structure and band gap were obtained from Ref. [44]. (b), (c) Band structure and partial DOS with SOC of $Cs_2AgBiCl_6$ with $d_{Ag-Cl}^{0,HSE(0.4)}$ calculated using the HSE(0.4)+SOC functionals.

Notably, the SOC has a significant impact on the band structure of $Cs_2AgBiCl_6$. Especially, the lowest conduction bands become much less dispersive after turning on SOC, resulting in an enlarged effective mass of the electrons. This is different from Pb-based perovskites, where SOC actually reduces the electron effective mass. The partial DOS [see Fig. 4(c)] analysis shows that the lowest conduction bands are made up mainly of Bi-6p states hybridized with Ag-5s and Cl-3p states, which split into two distinct peaks upon including SOC. Shi and Du proposed that the flat conduction bands in the Bi-based HDPs is due to the large electronegativity difference among cations and the large nearest-neighbor distances in cation sublattices [57]. Savory *et al.* argued that the flat conduction band is due to a mismatch in angular momentum of the frontier atomic orbitals of the B and B' ions [23]. Here we show that SOC also plays a crucial role for inducing the flat conduction bands in the Bi-based HDPs.

Regarding the impact of the SOC on the geometries, it has also been shown that structural optimization using HSE with SOC is important for proper descriptions of defect states in halide perovskites [58]. In the present case, we checked that the bond lengths of $Cs_2AgBiCl_6$ obtained with or without SOC are both 2.696 Å, indicating that the SOC effect has no impact on the geometries. Therefore, performing HSE(0.4)+SOC calculations based on the optimized structure using HSE(0.4) is a legitimate procedure.

The band structures of $Cs_2NaBiCl_6$ and $Cs_2AgBiBr_6$ have very similar features to those of $Cs_2AgBiCl_6$. Detailed results for these two materials are given in the SM (Figs. S3 and S4).

All the above results and analysis are based on the experimental lattice constants. The same calculations were also carried out for fully relaxed structures for each material. The obtained lattice constants, bond lengths, and corresponding band gaps with and without SOC corrections are presented in Tables S9–S12, respectively. From these results, the same behaviors can be observed, and thus the analysis performed above carries over to full relaxed geometries directly.

IV. SUMMARY

In this paper, we investigate the geometrical and electronic structures of $Cs_2BB'X_6$ (with B = Ag, Na, B' = In, Bi, and X = Cl, Br) HDPs via DFT calculations under different approximations to the XC functional. It is found that the commonly used computational protocol, i.e., performing band-structure calculations using HSE-type hybrid functionals on top of geometries determined by semilocal functionals, is not adequate for some of these materials, in particular, for In-based HDPs. Hybrid functionals incorporating appropriate portions of exact exchange can provide a satisfactory description of both the geometries and band gaps for this class of materials. This is because the B-X and B'-X bond lengths are sensitive to the employed functionals, and the VBM and CBM of the materials in turn depend almost linearly on the B-X (or B'-X) bond length. An in-depth analysis reveals that the determined equilibrium B-X (or, equivalently, B'-X) bond length is strongly correlated with the delocalization errors of these functionals, and moreover the change of the band edges with respect to the bond length is mostly governed by the variation of the hybridization strength between the frontier orbitals of B' and X. We show that the underlying driving mechanism of the intriguing behavior of the structural and electronic properties of the HDPs can already be understood via a simply linear three-atom B-X-B' molecular model. In practical calculations, it is advised that one should start with local-density approximation (LDA) and GGA, which typically underestimate and overestimate the lattice parameters, for structure relaxations to get initial ideas. If the electronic-structure properties obtained using LDA and GGA structures show large variation, it is then worthwhile to check what happens by relaxing the geometries using a consistent approach at the level of hybrid functionals.

Our paper provides an analysis framework and a practical guide for choosing appropriate functionals to reliably describe HDP materials. From the application point of view, we remark that the sensitivity of band gaps of the HDPs to their geometries offers a promising path for band structure engineering by doping and alloying.

ACKNOWLEDGMENTS

We acknowledge the funding support by the National Natural Science Foundation of China Grants No. 12134012, No.

12374067, and No. 12188101. This paper was also supported by the Strategic Priority Research Program of Chinese Academy of Sciences under Grant No. XDB0500201 and by the National Key Research and Development Program of China (Grants No. 2022YFA1403800 and No. 2023YFA1507004). The numerical calculations in this paper were carried out on the USTC HPC facilities and on the ORISE Supercomputer.

[1] H. Oga, A. Saeki, Y. Ogomi, S. Hayase, and S. Seki, Improved understanding of the electronic and energetic landscapes of perovskite solar cells: High local charge carrier mobility, reduced recombination, and extremely shallow traps, J. Am. Chem. Soc. **136**, 13818 (2014).

[2] S. D. Stranks, G. E. Eperon, G. Grancini, C. Menelaou, M. J. P. Alcocer, T. Leijtens, L. M. Herz, A. Petrozza, and H. J. Snaith, Electron-hole diffusion lengths exceeding 1 micrometer in an organometal trihalide perovskite absorber, Science **342**, 341 (2013).

[3] G. Xing, N. Mathews, S. Sun, S. S. Lim, Y. M. Lam, M. Grätzel, S. Mhaisalkar, and T. C. Sum, Long-range balanced electron- and hole-transport lengths in organic-inorganic $CH_3NH_3PbI_3$, Science **342**, 344 (2013).

[4] Q. Dong, Y. Fang, Y. Shao, P. Mulligan, J. Qiu, L. Cao, and J. Huang, Electron-hole diffusion lengths $>175\,\mu$m in solution-grown $CH_3NH_3PbI_3$ single crystals, Science **347**, 967 (2015).

[5] D. Shi, V. Adinolfi, R. Comin, M. Yuan, E. Alarousu, A. Buin, Y. Chen, S. Hoogland, A. Rothenberger, K. Katsiev *et al.*, Low trap-state density and long carrier diffusion in organolead trihalide perovskite single crystals, Science **347**, 519 (2015).

[6] S. De Wolf, J. Holovsky, S.-J. Moon, P. Löper, B. Niesen, M. Ledinsky, F.-J. Haug, J.-H. Yum, and C. Ballif, Organometallic halide perovskites: Sharp optical absorption edge and its relation to photovoltaic performance, J. Phys. Chem. Lett. **5**, 1035 (2014).

[7] NREL, Best research-cell efficiencies chart, https://www.nrel.gov/pv/cell-efficiency.html.

[8] G. Volonakis, A. A. Haghighirad, R. L. Milot, W. H. Sio, M. R. Filip, B. Wenger, M. B. Johnston, L. M. Herz, H. J. Snaith, and F. Giustino, $Cs_2InAgCl_6$: A new lead-free halide double perovskite with direct band gap, J. Phys. Chem. Lett. **8**, 772 (2017).

[9] J. Luo, X. Wang, S. Li, J. Liu, Y. Guo, G. Niu, L. Yao, Y. Fu, L. Gao, Q. Dong *et al.*, Efficient and stable emission of warm-white light from lead-free halide double perovskites, Nature (London) **563**, 541 (2018).

[10] J. Zhou, X. Rong, P. Zhang, M. S. Molokeev, P. Wei, Q. Liu, X. Zhang, and Z. Xia, Manipulation of Bi^{3+}/In^{3+} transmutation and Mn^{2+}-doping effect on the structure and optical properties of double perovskite $Cs_2NaBi_{1-x}In_xCl_6$, Adv. Opt. Mater. **7**, 1801435 (2019).

[11] W. Ning, X.-G. Zhao, J. Klarbring, S. Bai, F. Ji, F. Wang, S. I. Simak, Y. Tao, X.-M. Ren, L. Zhang, W. Huang, I. A. Abrikosov, and F. Gao, Thermochromic lead–free halide double perovskites, Adv. Funct. Mater. **29**, 1807375 (2019).

[12] J. D. Majher, M. B. Gray, T. A. Strom, and P. M. Woodward, $Cs_2NaBiCl_6 : Mn^{2+}$—A new orange-red halide double perovskite phosphor, Chem. Mater. **31**, 1738 (2019).

[13] C. J. Bartel, J. M. Clary, C. Sutton, D. Vigil-Fowler, B. R. Goldsmith, A. M. Holder, and C. B. Musgrave, Inorganic halide double perovskites with optoelectronic properties modulated by sublattice mixing, J. Am. Chem. Soc. **142**, 5135 (2020).

[14] L. Zhou, Y.-F. Xu, B.-X. Chen, D.-B. Kuang, and C.-Y. Su, Synthesis and photocatalytic application of stable lead-free $Cs_2AgBiBr_6$ perovskite nanocrystals, Small **14**, 1703762 (2018).

[15] X.-G. Zhao, D. Yang, Y. Sun, T. Li, L. Zhang, L. Yu, and A. Zunger, Cu–In halide perovskite solar absorbers, J. Am. Chem. Soc. **139**, 6718 (2017).

[16] E. Greul, M. Petrus, A. Binek, P. Docampo, and T. Bein, Highly stable, phase pure $Cs_2AgBiBr_6$ double perovskite thin films for optoelectronic applications, J. Mater. Chem. A **5**, 19972 (2017).

[17] W. Gao, C. Ran, J. Xi, B. Jiao, W. Zhang, M. Wu, X. Hou, and Z. Wu, High-quality $Cs_2AgBiBr_6$ double perovskite film for lead-free inverted planar heterojunction solar cells with 2.2% efficiency, ChemPhysChem **19**, 1696 (2018).

[18] M. Pantaler, K. T. Cho, V. I. E. Queloz, I. García Benito, C. Fettkenhauer, I. Anusca, M. K. Nazeeruddin, D. C. Lupascu, and G. Grancini, Hysteresis-free lead-free double-perovskite solar cells by interface engineering, ACS Energy Lett. **3**, 1781 (2018).

[19] G. Volonakis, M. R. Filip, A. A. Haghighirad, N. Sakai, B. Wenger, H. J. Snaith, and F. Giustino, Lead-free halide double perovskites via heterovalent substitution of noble metals, J. Phys. Chem. Lett. **7**, 1254 (2016).

[20] J. P. Perdew, K. Burke, and M. Ernzerhof, Generalized gradient approximation made simple, Phys. Rev. Lett. **77**, 3865 (1996).

[21] S. Adhikari and P. Johari, Theoretical insights into monovalent-metal-cation transmutation effects on lead-free halide double perovskites for optoelectronic applications, Phys. Rev. Mater. **7**, 075401 (2023).

[22] R.-I. Biega, Y. Chen, M. R. Filip, and L. Leppert, Chemical mapping of excitons in halide double perovskites, Nano Lett. **23**, 8155 (2023).

[23] C. N. Savory, A. Walsh, and D. O. Scanlon, Can Pb-free halide double perovskites support high-efficiency solar cells? ACS Energy Lett. **1**, 949 (2016).

[24] J. Zhou, Z. Xia, M. S. Molokeev, X. Zhang, D. Peng, and Q. Liu, Composition design, optical gap and stability investigations of lead-free halide double perovskite $Cs_2AgInCl_6$, J. Mater. Chem. A **5**, 15031 (2017).

[25] K. R. Bryenton, A. A. Adeleke, S. G. Dale, and E. R. Johnson, Delocalization error: The greatest outstanding challenge in density–functional theory, WIREs Comput. Mol. Sci. **13**, e1631 (2022).

[26] J. P. Perdew, A. Ruzsinszky, G. I. Csonka, O. A. Vydrov, G. E. Scuseria, L. A. Constantin, X. Zhou, and K. Burke, Restoring the density-gradient expansion for exchange in solids and surfaces, Phys. Rev. Lett. **100**, 136406 (2008).

[27] V. I. Anisimov, J. Zaanen, and O. K. Andersen, Band theory and Mott insulators: Hubbard *U* instead of Stoner *I*, Phys. Rev. B **44**, 943 (1991).

[28] J. Sun, A. Ruzsinszky, and J. P. Perdew, Strongly constrained and appropriately normed semilocal density functional, Phys. Rev. Lett. **115**, 036402 (2015).

[29] J. Heyd, G. E. Scuseria, and M. Ernzerhof, Hybrid functionals based on a screened Coulomb potential, J. Chem. Phys. **118**, 8207 (2003).

[30] A. V. Krukau, O. A. Vydrov, A. F. Izmaylov, and G. E. Scuseria, Influence of the exchange screening parameter on the performance of screened hybrid functionals, J. Chem. Phys. **125**, 224106 (2006).

[31] M. Chen, G. Guo, and L. He, Systematically improvable optimized atomic basis sets for ab initio calculations, J. Phys.: Condens. Matter **22**, 445501 (2010).

[32] P. Li, X. Liu, M. Chen, P. Lin, X. Ren, L. Lin, C. Yang, and L. He, Large-scale ab initio simulations based on systematically improvable atomic basis, Comput. Mater. Sci. **112**, 503 (2016).

[33] The abacus website, http://abacus.ustc.edu.cn.

[34] X. Qu, P. Xu, H. Jiang, L. He, and X. Ren, DFT+U within the framework of linear combination of numerical atomic orbitals, J. Chem. Phys. **156**, 234104 (2022).

[35] R. Liu, D. Zheng, X. Liang, X. Ren, M. Chen, and W. Li, Implementation of the meta-GGA exchange-correlation functional in numerical atomic orbital basis: With systematic testing on SCAN, rSCAN, and r^{2}SCAN functionals, J. Chem. Phys. **159**, 074109 (2023).

[36] P. Lin, X. Ren, and L. He, Accuracy of localized resolution of the identity in periodic hybrid functional calculations with numerical atomic orbitals, J. Phys. Chem. Lett. **11**, 3082 (2020).

[37] P. Lin, X. Ren, and L. He, Efficient hybrid density functional calculations for large periodic systems using numerical atomic orbitals, J. Chem. Theory Comput. **17**, 222 (2021).

[38] Y. Ji, P. Lin, X. Ren, and L. He, Reproducibility of hybrid density functional calculations for equation-of-state properties and band gaps, J. Phys. Chem. A **126**, 5924 (2022).

[39] M. Schlipf and F. Gygi, Optimization algorithm for the generation of ONCV pseudopotentials, Comput. Phys. Commun. **196**, 36 (2015).

[40] D. R. Hamann, Optimized norm-conserving Vanderbilt pseudopotentials, Phys. Rev. B **88**, 085117 (2013).

[41] P. Lin, X. Ren, and L. He, Strategy for constructing compact numerical atomic orbital basis sets by incorporating the gradients of reference wavefunctions, Phys. Rev. B **103**, 235131 (2021).

[42] F. Birch, Finite elastic strain of cubic crystals, Phys. Rev. **71**, 809 (1947).

[43] A. Noculak, V. Morad, K. M. McCall, S. Yakunin, Y. Shynkarenko, M. Wörle, and M. V. Kovalenko, Bright blue and green luminescence of Sb(III) in double perovskite Cs_2MInCl_6 (M = Na, K) matrices, Chem. Mater. **32**, 5118 (2020).

[44] E. T. McClure, M. R. Ball, W. Windl, and P. M. Woodward, Cs_2AgBiX_6 (X = Br, Cl): New visible light absorbing, lead-free halide perovskite semiconductors, Chem. Mater. **28**, 1348 (2016).

[45] A. H. Slavney, T. Hu, A. M. Lindenberg, and H. I. Karunadasa, A bismuth-halide double perovskite with long carrier recombination lifetime for photovoltaic applications, J. Am. Chem. Soc. **138**, 2138 (2016).

[46] L. Morrs and W. Robinson, Crystal structure of $Cs_2NaBiCl_6$, Acta Crystallogr. B **28**, 653 (1972).

[47] S. Grimme, J. Antony, S. Ehrlich, and H. Krieg, A consistent and accurate ab initio parametrization of density functional dispersion correction (DFT-D) for the 94 elements H-Pu, J. Chem. Phys. **132**, 154104 (2010).

[48] J. Sun, R. C. Remsing, Y. Zhang, Z. Sun, A. Ruzsinszky, H. Peng, Z. Yang, A. Paul, U. Waghmare, X. Wu *et al.*, Accurate first-principles structures and energies of diversely bonded systems from an efficient density functional, Nat. Chem. **8**, 831 (2016).

[49] Y. Zhang, J. Sun, J. P. Perdew, and X. Wu, Comparative first-principles studies of prototypical ferroelectric materials by LDA, GGA, and SCAN meta-GGA, Phys. Rev. B **96**, 035143 (2017).

[50] A. J. Cohen, P. Mori-Sánchez, and W. Yang, Insights into current limitations of density functional theory, Science **321**, 792 (2008).

[51] D. Hait and M. Head-Gordon, Delocalization errors in density functional theory are essentially quadratic in fractional occupation number, J. Phys. Chem. Lett. **9**, 6280 (2018).

[52] J. P. Perdew, R. G. Parr, M. Levy, and J. L. Balduz, Density-functional theory for fractional particle number: Derivative discontinuities of the energy, Phys. Rev. Lett. **49**, 1691 (1982).

[53] See Supplemental Material at http://link.aps.org/supplemental/10.1103/PhysRevResearch.6.033172 for the structural dependence of the band edges, as well as the effective masses, fully relaxed structures, and corresponding band gaps of all perovskites. Also contained are the electronic structures of $Cs_2NaInCl_6$, $Cs_2NaBiCl_6$, and $Cs_2AgBiBr_6$, the SOC effect of $Cs_2AgInCl_6$ and $Cs_2NaInCl_6$, and extended computational details.

[54] P. Han, X. Mao, S. Yang, F. Zhang, B. Yang, D. Wei, W. Deng, and K. Han, Lead-free sodium-indium double perovskite nanocrystals through doping silver cations for bright yellow emission, Angew. Chem. Int. Ed. **58**, 17231 (2019).

[55] R. Zeng, L. Zhang, Y. Xue, B. Ke, Z. Zhao, D. Huang, Q. Wei, W. Zhou, and B. Zou, Highly efficient blue emission from self-trapped excitons in stable Sb^{3+}-doped $Cs_2NaInCl_6$ double perovskites, J. Phys. Chem. Lett. **11**, 2053 (2020).

[56] L. Leppert, Excitons in metal-halide perovskites from first-principles many-body perturbation theory, J. Chem. Phys. **160**, 050902 (2024).

[57] H. Shi and M.-H. Du, Discrete electronic bands in semiconductors and insulators: Potential high-light-yield scintillators, Phys. Rev. Appl. **3**, 054005 (2015).

[58] X. Zhang, M. E. Turiansky, J.-X. Shen, and C. G. Van de Walle, Iodine interstitials as a cause of nonradiative recombination in hybrid perovskites, Phys. Rev. B **101**, 140101(R) (2020).